MOLECULAR AND CELLULAR BIOLOGY, Aug. 2011, p. 3497–3510 Vol. 31, No. 16
0270-7306/11/$12.00 doi:10.1128/MCB.01421-10

The Ras Inhibitors Caveolin-1 and Docking Protein 1 Activate Peroxisome Proliferator-Activated Receptor γ through Spatial Relocalization at Helix 7 of Its Ligand-Binding Domain▽

Elke Burgermeister,[1]* Teresa Friedrich,[2] Ivana Hitkova,[2] Ivonne Regel,[2] Henrik Einwächter,[2] Wolfgang Zimmermann,[3] Christoph Röcken,[4] Aurel Perren,[5] Matthew B. Wright,[6] Roland M. Schmid,[2] Rony Seger,[7] and Matthias P. A. Ebert[1]

Department of Medicine II, Universitätsklinikum Mannheim, Universität Heidelberg, Mannheim,[1] Department of Medicine II, Klinikum Rechts der Isar, Technische Universität München, Munich,[2] Tumor Immunology Laboratory, LIFE Center, Klinikum Universität München, München,[3] and Department of Pathology, Universität Kiel, Kiel,[4] Germany; Department of Pathology, Universität Bern, Bern,[5] and F. Hoffmann-La Roche, Basel,[6] Switzerland; and Department of Biological Regulation, The Weizmann Institute of Science, Rehovot, Israel[7]

Received 15 December 2010/Returned for modification 28 January 2011/Accepted 6 June 2011

Peroxisome proliferator-activated receptor γ (PPARγ) is a transcription factor that promotes differentiation and cell survival in the stomach. PPARγ upregulates and interacts with caveolin-1 (Cav1), a scaffold protein of Ras/mitogen-activated protein kinases (MAPKs). The cytoplasmic-to-nuclear localization of PPARγ is altered in gastric cancer (GC) patients, suggesting a so-far-unknown role for Cav1 in spatial regulation of PPARγ signaling. We show here that loss of Cav1 accelerated proliferation of normal stomach and GC cells *in vitro* and *in vivo*. Downregulation of Cav1 increased Ras/MAPK-dependent phosphorylation of serine 84 in PPARγ and enhanced nuclear translocation and ligand-independent transcription of PPARγ target genes. In contrast, Cav1 overexpression sequestered PPARγ in the cytosol through interaction of the Cav1 scaffolding domain (CSD) with a conserved hydrophobic motif in helix 7 of PPARγ's ligand-binding domain. Cav1 cooperated with the endogenous Ras/MAPK inhibitor docking protein 1 (Dok1) to promote the ligand-dependent transcriptional activity of PPARγ and to inhibit cell proliferation. Ligand-activated PPARγ also reduced tumor growth and upregulated the Ras/MAPK inhibitors Cav1 and Dok1 in a murine model of GC. These results suggest a novel mechanism of PPARγ regulation by which Ras/MAPK inhibitors act as scaffold proteins that sequester and sensitize PPARγ to ligands, limiting proliferation of gastric epithelial cells.

Peroxisome proliferator-activated receptor γ (PPARγ) belongs to the nuclear receptor (NR) superfamily (31). Infection by *Helicobacter pylori* is a major risk factor for gastric cancer (GC) in humans (68). *H. pylori* increases the expression of PPARγ, cytokines, and eicosanoids, while PPARγ protects the gastric epithelium by inhibiting apoptosis of host cells (19) and inflammation (42). PPARγ ligands (glitazones; 15-deoxy-prostaglandin J_2) have been shown to inhibit proliferation and induce growth arrest or apoptosis in human GC cell lines (32, 52, 53). PPARγ knockout (KO) mice are susceptible to chemically induced gastric carcinogenesis (36). In humans, the common "partial loss of function" gene polymorphism (Pro12Ala) is correlated with an increased risk of GC, suggesting a role for PPARγ as a tumor suppressor in the stomach (67).

PPARγ inhibits cell proliferation by several mechanisms, including inhibition of cyclin D1 expression, promotion of its proteasomal degradation, and upregulation of cyclin-dependent kinase (CDK) inhibitors (20, 55, 65). Members of the Ras/mitogen-activated protein kinase (MAPK) cascade, such as extracellular signal-regulated kinases 1/2 (ERK1/2), counteract this effect by inducing cyclin D1 expression and reducing PPARγ activity by phosphorylation on serine 84 (serine 82 in mouse) in its N-terminal activation function (AF1) (7). Cav1, a scaffold protein of plasma membrane caveolae (46), attenuates ERK1/2 activation and cell growth by sequestration of upstream MAPK cascade components, including growth factor receptors, Ras, Raf, and MEK1. In contrast, Cav1-null cells or tissues from Cav1-deficient animals show increased proliferation with hyperactivation of ERK1/2, e.g., in crypts of the colon and in mammary glands (33, 50). Moreover, since both PPARγ and Cav1 are markers of terminally differentiated cells, such as in macrophages and adipocytes (31, 46), we hypothesize that Cav1 and PPARγ collaborate to regulate cell proliferation.

Nonnuclear compartmentalization of NR proteins has been shown to contribute to their functional inactivation in human cancers. Signal-mediated shuttling of PPARγ between the nucleus and the cytoplasm has been described in several *in vitro* systems (as reviewed in reference 7). PPARγ itself facilitates subcellular translocation of nuclear factor-kappa B in intestinal epithelial cells (28) and protein kinase C in macrophages (61). Redistribution of PPARγ has also been described to occur in human GC (21, 45). PPARγ resides in the nucleus in the normal gastric mucosa but is primarily cytoplasmic in intestinal metaplastic (IM) epithelium, a putative preneoplastic

* Corresponding author. Mailing address: Department of Medicine II, Universitätsklinikum Mannheim, Theodor-Kutzer Ufer 1-3, Universität Heidelberg, D-68167 Mannheim, Germany. Phone: 49 621 383 3284. Fax: 49 621 383 3805. E-mail: elke.burgermeister@lrz.tum.de.
▽ Published ahead of print on 20 June 2011.

lesion in GC. The high cytoplasmic-to-nuclear expression ratio of PPARγ in IM decreases during progression of primary differentiated GC to undifferentiated, metastatic gastric tumors, where PPARγ reappears in the nucleus. However, the physiological significance and molecular players that govern regulation of PPARγ by subcellular redistribution have not been studied.

We have shown previously (i) that PPARγ's transcriptional activity is inhibited by its nuclear export through the mitogen-activated protein kinase (MAPK) kinase MEK1 (4, 6, 7), (ii) that PPARγ interacts with and transcriptionally upregulates Cav1 (8), (iii) and that Cav1 is expressed in human GC, inhibits proliferation, and promotes survival of human GC cells under stress (9). In the present study, we have elucidated the mechanism and functional consequences of subcellular redistribution of PPARγ by Cav1 in GC. We explored Cav1 deficiency and PPARγ activation in the normal stomach and in GC of mice and by employing overexpression or RNA interference (RNAi)-mediated knockdown approaches in human GC cells. Our data indicate that the Ras/MAPK inhibitors Cav1 and docking protein 1 (Dok1) inhibit proliferation of gastric epithelial cells by potentiating the ligand sensitivity of PPARγ.

MATERIALS AND METHODS

Subjects. Tissue specimens from GC patients were collected, stored, and classified histologically according to the Laurén method (9, 66). The study protocol was approved by the Ethics Committee of the Technische Universität München.

Animals. Homozygous Cav1 knockout (CAV-KO) (strain Cav1tm1Mls/J; stock no. 004585) and matched control wild-type (WT) (strain B6129SF2/J; stock no. 101045) C57BL/6J mice were obtained from the Jackson Laboratory (Bar Harbor, ME) and maintained on a mixed background. *In vivo* labeling with bromodeoxyuridine (BrdU) was performed as published previously (66). Transgenic CEA424-SV40 T-antigen (Tag) (59) mice were maintained on a pure C57BL/6N background. The Tag mice ($n = 5$ per group) received a chow diet or a chow diet (both from Altromin, Lage, Germany) supplemented with 0.02% (wt/wt) rosiglitazone (ROSI) (30) (Chemos, GmbH, Regenstauf, Germany) for 6 weeks (approximately 25 mg/kg of body weight/day). Animal studies were conducted under the ethical guidelines of the Technische Universität München and approved by the appropriate government authorities.

Reagents. The chemicals were from Merck (Darmstadt, Germany) or Sigma (Taufkirchen, Germany). Rosiglitazone was provided by F. Hoffmann La Roche AG (Basel, Switzerland). The rabbit polyclonal antisera were Cav1 (N-20; sc-894; Santa Cruz Biotechnology, CA), PPARγ (H-100; sc-7196), Phospho-serine 82/84 PPARγ (AW504; Upstate/Millipore, GmbH, Schwalbach, Germany), PPARγ (C26H12; no. 2435) and phosphothreonine/tyrosine-ERK1/2 (p44/p42) (no. 4370) (both from Cell Signaling, Danvers, MA), Ki-67 (SP6; DCS, GmbH, Hamburg, Germany), Hsp90α/β (H-114; sc-7947), furin (H-220; sc-20801), and lamin A/C (H-110; sc-20681). The mouse monoclonal antibodies (Abs) were Dok1 (A-3; sc-6929), PPARγ (E-8; sc-7273), MEK1 (H-8; sc-6250), Cav1 (no. 2297; BD/Transduction Laboratories, San Jose, CA), cyclin D1 (A-12; sc-8396), and β-actin (AC74; Sigma). Pan-cytokeratin (CK) antibody was from Dako (Hamburg, Germany). The Dok1 small interfering RNA (siRNA) oligonucleotides were from Dharmacon (Thermo-Fisher Scientific, Waltham, MA). Cell-permeable peptides (18) were synthesized (Thermo-Fisher Scientific) with a header comprising the antennapedia internalization sequence RQIKIWFQNR RMKWKK (AP) alone or fused to the human Cav1 scaffolding domain (CSD), amino acids (aa) 82 to 101 (RQIKIWFQNRRMKWKK-DGIWKASFTTFTVT KYWFYR) (AP-Cav1).

DNA constructs. The expression and reporter plasmids employed were green fluorescent protein (GFP)-PPARγ and 3xPPRE(ACO)-pTK-luc, as described previously (5). Deletion of aa 92 to 98 from the Cav1 scaffolding domain (CSD; aa 82 to 101) in the pcDNA3-Cav1 full-length cDNA and aa 58 to 63 (ΔH7/2) and 66 to 72 (ΔH7/1) in the putative Cav1-binding motif within helix 7 (H7) of the ligand-binding domain (LBD) in GFP-PPARγ was performed using site-directed mutagenesis (QuikChange kit; Stratagene, Amsterdam, Netherlands). Full-length p62 Dok1 cDNA was cloned from SW480 human colon adenocarcinoma cells and inserted into pTarget vector (Promega, GmbH, Mannheim, Germany). The mammalian 2-hybrid system (Stratagene) was performed as published previously (9), using full-length Cav1 cDNA in pCMV-AD (Stratagene). Transient-transfection and luciferase assays were performed as described previously (9).

Cell culture. Human embryonic kidney HEK293, colon adenocarcinoma SW480, and parental GC cell lines (all from the American Type Culture Collection, Rockville, MD) and stably transfected AGS and MKN45 clones were maintained as previously described (9).

Proliferation assays. MTT [3-(4,5-dimethyl-2-thiazolyl)-2,5-diphenyl-2H-tetrazolium bromide] and BrdU assays were performed according to the manufacturer's protocols (Roche Diagnostics, GmbH, Mannheim, Germany). For "mitotic shake-off," AGS cells were seeded in 15-cm dishes and grown to subconfluency (50 to 70%) for 48 to 72 h before addition of Dulbecco's modified Eagle's medium (DMEM) containing 20% (vol/vol) fetal calf serum (FCS) for 24 h followed by 0.25 μg/ml Colcemid in DMEM enriched with 20% (vol/vol) FCS overnight. G_2-arrested cells were detached by gentle tapping and collected by centrifugation, washed twice with DMEM containing 10% (vol/vol) FCS, and reseeded into 24-well plates (5×10^5 per well for RNA extraction) or 96-well plates (2,000 per well for BrdU uptake).

Immunofluorescence, CoIP, and WB. Staining was performed in triple-color mode visualizing DAPI (4′,6-diamidino-2-phenylindole) and Alexa-488 and -594 using a digital camera-connected (Axiovision, release 4.4) fluorescence microscope (Axiovert 200 M; Carl Zeiss MicroImaging, GmbH, Hallbergmoos, Germany) as described previously (9). Coimmunoprecipitation (CoIP) and Western blotting (WB) were done as described previously (9).

Subcellular fractionation. Hypotonic lysis was performed in 1 ml of HL buffer (20 mM HEPES, pH 7.4, 2 mM EGTA, 2 mM $MgCl_2$, 1 mM sodium orthovanadate, 1 mM dithiothreitol, Complete protease inhibitor) on ice. Cells were scraped and homogenized by repeated pipetting and incubated on ice for 30 min, followed by a 5-min centrifugation at 7,000 rpm at 4°C to recover the supernatant (cytosol). Nuclei were extracted for 30 min on ice in 150 μl of HS buffer (HL buffer supplemented with 450 mM NaCl) with frequent vortexing, followed by a 10-min centrifugation at full speed at 4°C to recover the supernatant (nuclear extract). Detergent-insoluble (Triton X-100) low-density membrane domains ("lipid rafts") and their associated proteins were purified by equilibrium density ultracentrifugation in sucrose gradients as published previously (8).

MS. Immunoprecipitates were separated by SDS-PAGE and detected by silver staining (kit by GE Healthcare, Munich, Germany). Protein lanes were cut and processed for matrix-assisted laser desorption ionization (MALDI)–mass spectrometry (MS) in α-cyano-4-hydroxycinnamic acid (CHCA) (Bruker, Bremen, Germany) as published previously (16). Mass spectra were acquired using a model 4700 proteomics analyzer (MALDI-tandem time of flight [TOF-TOF]) mass spectrometer (Applied Biosystems, Framingham, MA). Measurements were performed with a 355-nm Nb:YAG laser in positive reflector mode with a 20-kV acceleration voltage. For each MS and tandem MS (MS-MS) spectrum, 3,000 shots were accumulated. For each spot on a MALDI plate, the eight most intense peptides were selected for additional MS-MS analysis. The acquired MS-MS spectra were searched against the UniRef100 databases using an in-house version of Mascot. The settings were as follows: taxon, human; enzyme, trypsin; fixed modification, carbamidomethylation; and variable modifications, oxidized methionine. The GPS Explorer 2 software program yielded the Mascot best ion score. The significance level for a peptide score was set to greater than 20 and that for a protein score to greater than 50 to 60.

Immunohistochemistry (IHC). Antibody and hematoxylin-eosin (H&E) stainings were performed as described previously (9, 66). Quantitative analysis of the frequency and intensity of Cav1 staining in human GC tissue microarrays was performed by the expert pathologist C. Röcken as published previously (9). The colorimetric substrates 3,3′-diamino benzidine (brown) and VectorRed (red) were used (Vectorlabs, Burlingame, CA).

DNA microarray, RT-PCR, and qPCR. AGS clones stably transfected with Cav1 (AGS/Cav1) or empty vector (AGS/EV) were treated with 1 μM rosiglitazone for 16 h. Total RNA (1 μg) was labeled with a one-cycle cRNA labeling kit (Affymetrix, Wycombe, United Kingdom) and hybridized to HGU133 Plus 2.0 arrays (Affymetrix). Gene signatures were identified using gene set enrichment analysis (GSEA) (66). Reverse transcription-PCR (RT-PCR) and quantitative PCR (qPCR) were performed as published previously (9).

Statistical analyses. Results are expressed as means ± standard errors (SE) for at least 5 animals per genotype or 3 independent experiments from different cell passages. Statistical analysis was performed using Graphpad Prism (version 4.0). P values (*, $P < 0.05$) were calculated using Student t and Mann Whitney tests.

RESULTS

Cav1 deficiency promotes proliferation of gastric epithelial cells *in vitro* and *in vivo*. We previously showed that Cav1 inhibits proliferation of human GC cell lines (9). In the present study, we explored the mechanism of growth inhibition by Cav1. Wild-type Cav1 (AGS/Cav1) or empty-vector (AGS/EV) plasmids were stably transfected into AGS cells, which are naturally devoid of Cav1 (9). Cells were released from Colcemid-induced G_2 arrest, and the kinetics of cell cycle reentry was measured by uptake of bromodeoxyuridine (BrdU). AGS/EV cells reentered the cell cycle at a faster time course (approximately 3 h) than AGS/Cav1 cells (Fig. 1A). This difference was also evident from an accelerated kinetic of cyclin D1 expression (Fig. 1B).

To assess whether Cav1 also inhibits proliferation *in vivo*, we characterized the gastric phenotype of Cav1 knockout (Cav1-KO) mice. Immunohistochemistry (IHC) on paraffin sections showed prominent Cav1 staining in the stomachs of wild-type (WT) mice within the lamina propria and submucosa in fat, smooth muscle and vessel walls (Fig. 1C). Staining for Cav1 was also detected in cross sections through the gastric corpus within the glandular epithelium. Interestingly, IHC against the proliferation marker Ki-67 (Fig. 1D) revealed that Cav1-KO stomachs show foveolar hyperplasia of gastric glands. The mucosa of the gastric corpus in Cav1-KO mice had elongated foveolae with dense nuclei compared to the more regularly spaced and shorter foveolae in WT mice. The frequencies of Ki-67 (Fig. 1E)- and BrdU (not shown)-positive nuclei in the mucus neck region of gastric glands were elevated in Cav1-KO mice compared to those in WT littermates. RT-qPCR analysis confirmed elevated *cyclin D1* mRNA levels in Cav1-KO mice (Fig. 1E). Thus, consistent with the *in vitro* studies, loss of Cav1 *in vivo* resulted in increased proliferation of gastric epithelial cells.

Localization of PPARγ in human GC tissue and cell lines. Prior evidence showing that (i) Cav1 and PPARγ inhibit cyclin D1 expression/function, (ii) Cav1 inhibits Ras/MAPKs, and (iii) PPARγ is inactivated by Ras/MAPKs prompted us to test the hypothesis that Cav1 functionally cooperates with PPARγ to limit cell proliferation. We first investigated the subcellular distribution of PPARγ in human GC specimens ($n = 10$) by IHC on paraffin sections (39) (Fig. 2A). In the normal gastric epithelium, PPARγ was primarily localized in the nucleus, a finding consistent both with its function as an NR and with previous studies (21, 45). In intestinal-type GC tissue with regions of intestinal metaplasia (IM), a predominantly cytoplasmic localization of PPARγ was observed in accordance with previous reports (21, 45). In contrast, nuclear PPARγ predominated in specimens of diffuse-type GC. We previously showed (9) that Cav1 is present in the glands of the normal human gastric mucosa and oriented toward the luminal side of intestinal metaplastic (IM) epithelium (Fig. 2A). Quantitative IHC on tissue microarrays of a larger series of GC patients ($n = 185$) confirmed the increase of cytosolic Cav1 in IM ($n = 58$) compared to the level for normal gastric tissue (Fig. 2B). These data suggest that a shift from nuclear to cytosolic PPARγ occurs upon malignant transformation of the gastric epithelium.

We then performed subcellular fractionation studies to de-

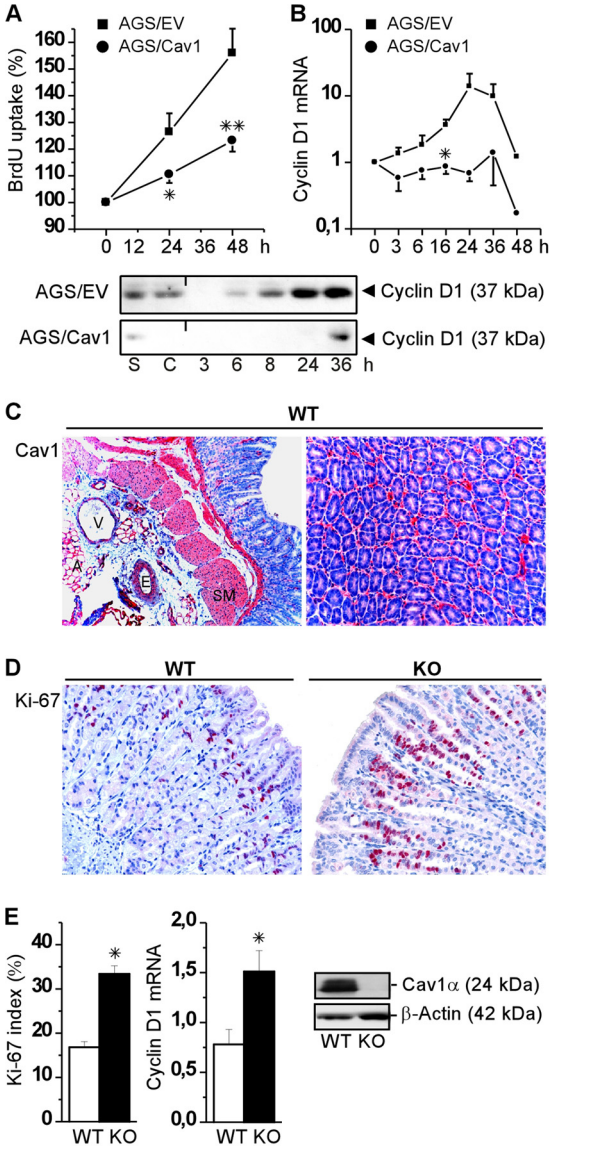

FIG. 1. Loss of gastric Cav1 promotes proliferation *in vitro* and *in vivo*. (A) BrdU uptake into synchronized AGS clones. Optical density (OD) values from enzyme-linked immunosorbent assays (ELISAs) were calculated as percentages ± SE ($n = 3$). *, $P < 0.05$ for AGS/EV versus AGS/Cav1. (B) Time course of cyclin D1 mRNA and protein expression upon release from G_2 arrest. (Top) Threshold cycle (C_T) values from RT-qPCRs were normalized to values for β2-microglobulin and calculated as fold changes ± SE ($n = 3$). *, $P < 0.05$ for AGS/EV versus AGS/Cav1. (Bottom) WB of whole-cell lysates. *s*, starved sample; *c*, control sample. (C) Cav1 in gastric mucosal and submucosal tissues of WT mice detected by IHC (red) using the monoclonal Ab on paraffin sections. (Left) Longitudinal section (V/E, vessel/endothelium; A, adipose; SM, smooth muscle). (Right) Cross section through glands of the gastric corpus. Magnifications, ×100 and ×200. (D) Cav1-deficient mice show foveolar hyperplasia of gastric glands as detected by IHC (red) against Ki-67. Magnification, ×200. (E) (Left) Proliferation index for Ki-67. The ratio of positive nuclei per foveola to total nuclei was calculated as the percentage ± SE ($n = 6$ per genotype). (Right) Gastric *cyclin D1* mRNA quantified by RT-qPCR. C_T values were normalized to the value for β2-microglobulin and calculated as fold changes ± SE ($n = 6$ per genotype). (Insert) Cav1 protein in tissue lysates from WT and Cav1-KO stomachs compared to β-actin. Representative Western Blots (WB) are shown. *, $P < 0.05$ for WT versus Cav1-KO.

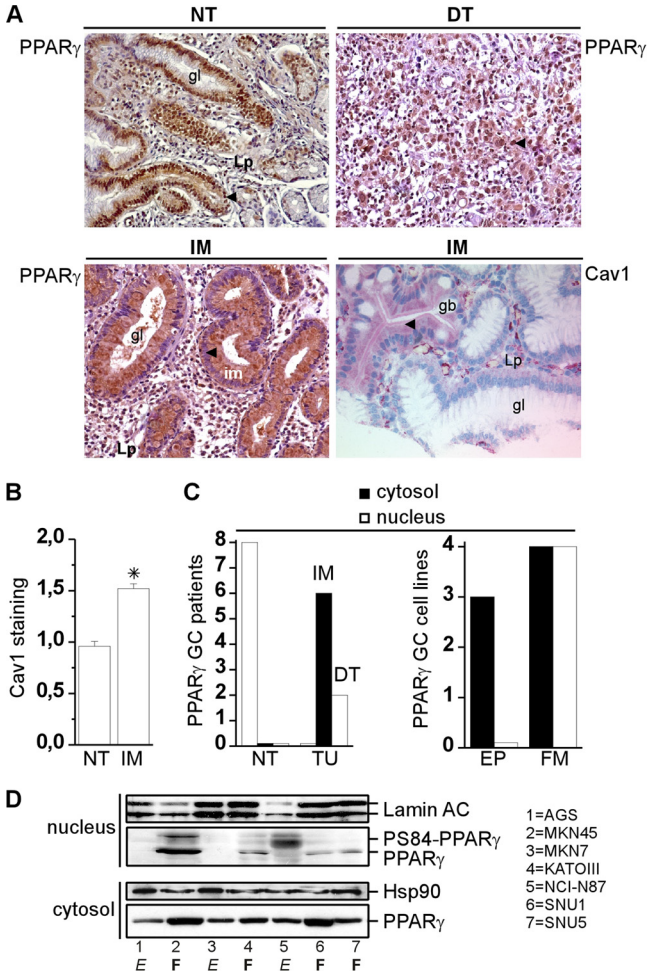

FIG. 2. Localization of PPARγ in human GC patient tissues and cell lines. (A) IHC on paraffin sections using the polyclonal Ab for PPARγ (brown) and the monoclonal Ab for Cav1 (red). NT, normal stomach; IM, intestinal metaplasia in intestinal-type GC; DT, diffuse-type GC; gl, gastric gland; Lp, lamina propria; gb, goblet cell. Arrows indicate nuclear staining for PPARγ (brown) in NT and DT in contrast to cytosolic staining for PPARγ (brown) and Cav1 (red) in IM. Magnifications, ×100 and ×200. (B) Quantitative analysis of IHC summarizing the enhanced expression of Cav1 in IM tissue compared to that in normal tissue. Combined scores for the intensity and frequency of Cav1 staining in tissue microarrays from GC patients are expressed as fold changes ± SE. *, $P < 0.05$ for IM ($n = 58$) versus NT ($n = 185$). (C) Cytoplasmic and nuclear localization of PPARγ in GC patients ($n = 10$) and parental GC cell lines ($n = 7$). P, GC cell lines derived from primary GC tissue; M, GC cell lines originating from GC metastases; E, GC cell lines with epithelial morphology; F, GC cell lines with fibroblast/spherical morphology. Absolute numbers of patients and cell lines are shown. Nuclear PPARγ predominated in NT/DT tissues and in FM cell lines. Cytosolic PPARγ was present in IM tissue and in all 7 GC cell lines tested (FM/EP). (D) Subcellular fractionation of 7 parental GC cell lines. Representative WBs detecting nuclear and cytosolic PPARγ using the polyclonal Ab, compared to lamin AC for nuclear and Hsp90 for cytosolic fractions. Lane numbers represent GC cell lines, and the legend is presented next to the gel.

termine the localization of PPARγ (Fig. 2C). In GC lines with adherent epithelial morphology, such as AGS, MKN7, and NCI-N87, PPARγ was primarily localized in the cytosol, whereas in the metastatic cell lines with mesenchymal fibroblast-like phenotypes, including MKN45, KATOIII, SNU1, and SNU5, PPARγ was also present in the nucleus (Fig. 2D). The observation that all GC cell lines expressed the bulk of PPARγ (the 50-kDa PPARγ1 isoform) in the cytosol is in line with the predominantly cytosolic distribution of PPARγ in tissue samples from GC patients. Based on these observations, we raised the hypothesis that Cav1 controls the subcellular distribution and activity of PPARγ.

Cav1 attenuates nuclear localization and ERK-dependent serine 84 phosphorylation of PPARγ. To test whether Cav1 influences the localization of PPARγ, we performed fractionation studies with AGS/Cav1 and AGS/EV cells. Following serum deprivation for 16 h, the cells were treated with the mitogenic Raf activator tetradecanoyl phorbol acetate (TPA) (100 nM) or the PPARγ agonist rosiglitazone (10 μM) for 0 to 90 min. In starved cells, the bulk of PPARγ remained in the cytosol (Fig. 3A). In general, AGS/EV cells exhibited more nuclear PPARγ than AGS/Cav1 cells, irrespective of treatment (Fig. 3B) (see Fig. S1 at http://www.gastric.de/typo3_mannheim/index.php?id=down000), suggesting that nuclear translocation of PPARγ is restricted by Cav1. Similar results were obtained from Cav1-transfected SW480 cells (not shown).

ERK1/2-mediated phosphorylation of PPARγ on serine 84 (S84) was detected by WB (15, 24). The 55- and 60-kDa phospho-PPARγ1 bands appeared in the nucleus but not in the cytosol (Fig. 3A). Both TPA and rosiglitazone increased S84 phosphorylation only in AGS/EV cells. Despite having lower absolute levels of nuclear PPARγ, interestingly, AGS/Cav1 cells had greater constitutive levels of S84-phosphorylated nuclear PPARγ than AGS/EV cells, suggesting phosphorylation independent of ERKs (11, 60–62) (Fig. 3B) (see Fig. S1 at http://www.gastric.de/typo3_mannheim/index.php?id=down000). The MEK1/2 inhibitor U0126 prevented TPA-induced PPARγ phosphorylation (data not shown), corroborating the participation of ERKs in this event. ERKs were activated by TPA and rosiglitazone, with higher amplitude and accelerated time course (peak at 5 min) in AGS/EV than in AGS/Cav1 cells (see Fig. S1 at the URL mentioned above). These data indicated that Cav1 promotes cytosolic sequestration and inhibits ERK-dependent, but not ERK-independent, phosphorylation of nuclear PPARγ.

Cytosolic sequestration of PPARγ by Cav1 inhibits basal and ligand-dependent transcription. If indeed Cav1 leads to retention of PPARγ in the cytoplasm, one may expect that Cav1-overexpressing cells are less responsive to transcriptional upregulation of PPARγ target genes upon treatment with PPARγ ligands. To test this, AGS clones were treated for 16 h with 1 μM rosiglitazone, and total RNA was hybridized to DNA microarrays (see Fig. S2 at http://www.gastric.de/typo3_mannheim/index.php?id=down000). Bioinformatic analysis (see Fig. S3 at the URL mentioned above) revealed that genes which contain PPARα/γ-responsive DNA elements (PPRE) in their promoters were specifically enriched in AGS/EV cells compared to the level in AGS/Cav1 cells (see Table S1 at the URL mentioned above). This gene set comprised enzymes in lipid metabolism, receptors for arachidonic acid metabolites, the adipogenic transcription factor C/EBPα, and PPARγ itself.

For validation of the microarray results, two cognate PPARγ target genes, the acyl coenzyme A (CoA) oxidase (ACO) and trefoil factor 2 (TFF2) genes (56), were measured by RT-

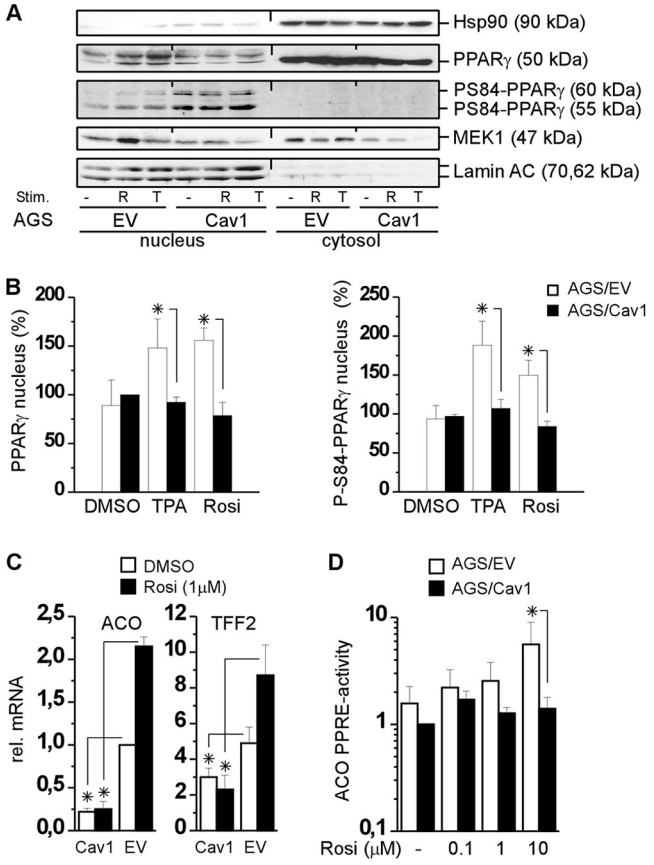

FIG. 3. Loss of Cav1 promotes nuclear localization and ERK-dependent phosphorylation of PPARγ at serine 84. (A, B) Subcellular fractionation. Serum-deprived AGS clones were stimulated for 60 min with TPA (100 nM) or rosiglitazone (10 μM). Representative WBs of cytosolic and nuclear fractions are shown. AGS/EV cells accumulate more general and serine 84 (S84)-phosphorylated PPARγ in the nucleus upon stimulation than AGS/Cav1 with constitutively phosphorylated PPARγ. Representative WBs (A) are presented together with results for quantitative densitometric analyses (B). OD values from bands in WB gels were normalized to values for nuclear lamin A/C and calculated as percentages ± SE ($n = 5$) of values for vehicle controls. *, $P < 0.05$ for AGS/EV versus AGS/Cav1. (C, D) Ectopic Cav1 promotes cytosolic sequestration and inhibits basal and ligand-dependent transcription of PPARγ target genes. (C) mRNA expression. AGS clones were incubated for 16 h with vehicle or 1 μM rosiglitazone. C_T values from RT-qPCRs were normalized to values for β2-microglobulin and calculated as fold changes ± SE ($n = 5$ per clone). *, $P < 0.05$ for Cav1 versus EV. (D) Transactivation. AGS clones were transiently transfected with 3xPPRE(ACO)pTK-luc reporter plasmid and treated for 24 h with rosiglitazone. Luciferase values normalized to protein content are indicated as fold changes ± SE ($n = 3$) compared to values for vehicle-treated controls. *, $P < 0.05$ for AGS/Cav1 versus AGS/EV.

qPCR. The mRNA levels of these genes were substantially reduced in AGS/Cav1 cells compared to the level in AGS/EV cells. Notably, both basal and ligand-dependent mRNA levels were elevated in AGS/EV cells and effectively suppressed in the presence of Cav1 (Fig. 3C). Similar results were obtained in transiently transfected SW480 cells, a cell line that also lacks endogenous Cav1 (data not shown). Lastly, we transiently transfected AGS clones with a reporter plasmid driven by three repeats of the human PPRE from the ACO gene in front of a basal herpes simplex virus-thymidine kinase (HSV-TK) promoter (Fig. 3D). Rosiglitazone upregulated the ACO reporter in AGS/EV cells but not in AGS/Cav1 cells. Taken together, these data show that cytosolic sequestration of PPARγ by Cav1 restricts nuclear accumulation of PPARγ, making it unavailable at promoters of target genes.

PPARγ associates with MEK1 and Cav1 in the cytosol. We previously showed that PPARγ is subject to rapid (5- to 60-min) nuclear export by MEK1, the upstream regulatory kinase of ERK1/2, after stimulation of cells with mitogens or PPARγ ligands (4, 6, 9). This interaction is mediated by direct binding of MEK1 to the C-terminal helix 12 (AF-2) of PPARγ's ligand-binding domain (LBD). To determine if Cav1 interferes with this event, we performed coimmunoprecipitation (CoIP) studies of PPARγ and MEK1 from cytosolic lysates of AGS clones (Fig. 4A). Serum-deprived cells had low levels of cytoplasmic MEK1-PPARγ complexes. TPA increased MEK1-PPARγ complex formation more efficiently in AGS/EV than in AGS/Cav1 cells, consistent with inhibition of the Ras/MAPK pathway by Cav1. In contrast, rosiglitazone preferentially promoted MEK1-PPARγ interaction in AGS/Cav1 cells, suggesting that ligand-activated PPARγ associates with both MEK1 and Cav1 in the cytosol.

We next asked whether MEK1 and Cav1 compete for the same binding site on PPARγ. An association of Cav1 and PPARγ (Fig. 4B, first lanes) was observed in CoIP experiments. Pulldown with control antibodies (second lanes) or empty beads confirmed the specificity of the reaction (third and fourth lanes). Stimulation with rosiglitazone increased the cytoplasmic localization of PPARγ in AGS/Cav1 cells (Fig. 4B). Equilibrium density ultracentrifugation (see Fig. S4 at http://www.gastric.de/typo3_mannheim/index.php?id=down000) confirmed that PPARγ, MEK1, and Cav1 colocalized within the cytosolic protein fractions (fractions 8 to 10), while the detergent-insoluble low-buoyant-density (lipid raft) fractions (fractions 4 to 6) contained the remaining PPARγ. These data indicated that PPARγ is bound to Cav1 and MEK1 in the cytosol and that these associations are not exclusive.

Helix 7 in the ligand-binding domain of PPARγ harbors a Cav1-binding motif. BLASTP and COMPLEX PATTERN SEARCH (http://www.dkfz.de/mga2) identified a putative Cav1-binding motif in helix 7 (H7) located in the ligand-binding domain (LBD) of human PPARγ1. This sequence is rich in aromatic amino acids $FX_7FX_2FX_4FXFX_3F$ (aa 350 to 372; Swiss-Prot accession no. P37231) (Fig. 4C) and resembles the consensus Cav-binding motif suggested by Couet et al. ($\phi X \phi X_4\phi$ and $\phi X_4\phi X_2\phi$, where ϕ is an aromatic amino acid such as tryptophan [W], phenylalanine [F], or tyrosine [Y]) (13, 14) in reverse orientation. This motif is well conserved in PPARγ, PPARβ/δ, and PPARα across different species, including humans, primates, rodents, and *Xenopus* (see Table S2 at http://www.gastric.de/typo3_mannheim/index.php?id=down000). Helix 7 is important for recruitment of NR coactivators (NRCoA) and stabilization of the holo-LBD of NRs (23). Importantly, helix 7 is independent of helix 12 (AF2), which harbors the steroid receptor coactivator-1 (SRC1) and MEK1 interaction sites (9, 44), and helix 10, which participates in heterodimerization with retinoic X receptor (RXR) (17) (Fig. 4C). Specific helix 7 residues have been implicated in

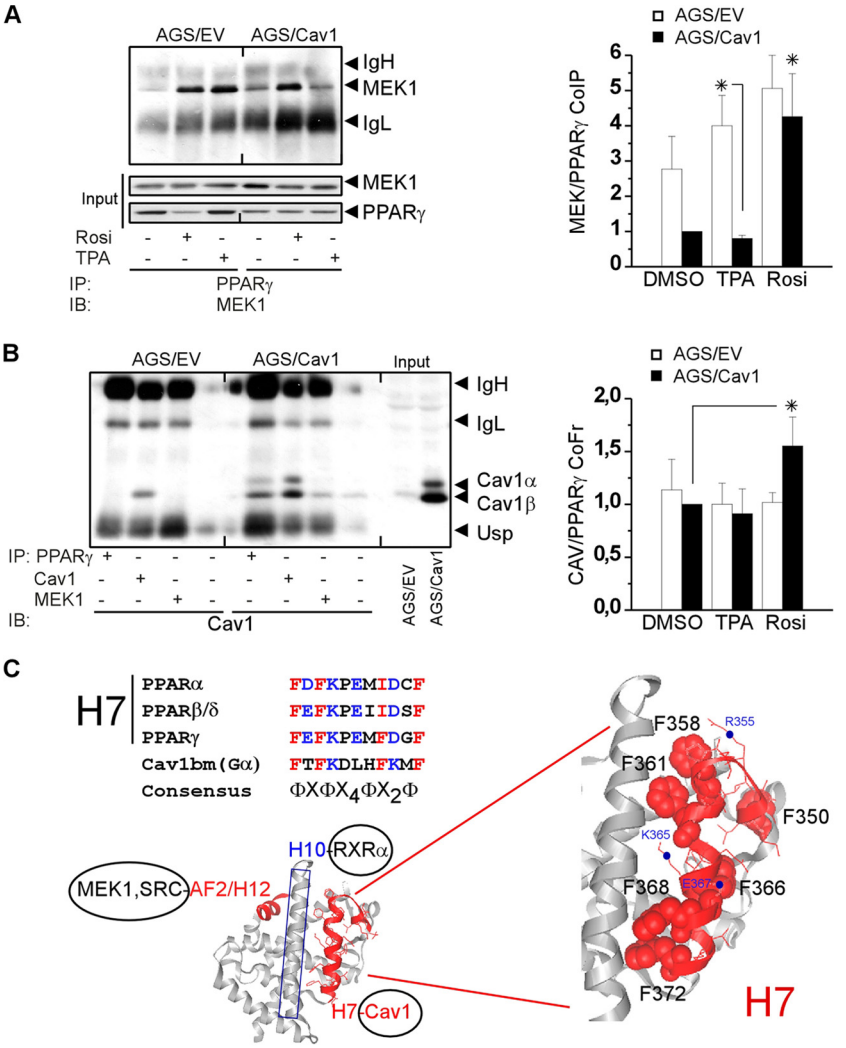

FIG. 4. PPARγ interacts with MEK1 and Cav1 in the cytosol. (A) PPARγ-MEK1 interaction. Serum-deprived AGS clones were stimulated for 30 min with TPA (100 nM) and rosiglitazone (10 μM) before CoIP (IP) from cytosolic lysates using the polyclonal PPARγ antiserum. Representative WBs and results for densitometric analyses are shown. OD values for CoIP-ed complexes were normalized to the input of corresponding proteins and calculated as fold changes ± SE ($n = 3$) compared to the value for the vehicle control. *, $P < 0.05$ for AGS/Cav1 versus AGS/EV; *, $P < 0.05$ for ROSI versus dimethyl sulfoxide (DMSO). IB, immunoblot. (B) PPARγ-Cav1 interaction. (Left) CoIP from cell lysates using polyclonal Abs (first to third lanes) or IgG controls (fourth lane). Representative WBs. (Right) Rosiglitazone increases cofractionation of Cav1 and PPARγ in the cytosol of AGS/Cav1 cells. OD values for WB bands detecting cytoplasmic PPARγ were normalized to values for Hsp90 and calculated as fold changes ± SE ($n = 3$) compared to the value for the vehicle control. *, $P < 0.05$ for ROSI versus DMSO. (C) Peptide motifs and three-dimensional (3D) interaction surfaces on the ligand-binding domain (LBD) of PPARγ. (Left) Alignment of the amino acid sequences of hydrophobic/aromatic Cav1-binding motifs (Cav1bm) in members of the PPAR family (alpha, beta/delta, and gamma) compared to the consensus sequence of Gα proteins (13, 14). Note the reverse (C-terminal to N-terminal) orientation of the amino acid sequence in PPARs. Red, aromatic/hydrophobic amino acids; blue, charged amino acids. (Right bottom) 3D ribbon models of surface-exposed amino acid residues in helix 7 (H7) of PPARγ's LBD, obtained using RASMOL. Red, H7 (Cav1-binding motif) and AF2/H12 (MEK1-NRCoA binding; ligand "charge clamp"); blue, H10 (heterodimerization interface).

several regulatory functions, including K365(γ1), a target for sumoylation (47), and F372(γ1), influencing ligand sensitivity during adipogenesis (64) and interaction with β-catenin (34). Several mutations in helix 7, such as R357X(γ1) (1) and F358/388L(γ1/2) (22), are associated with lipodystrophy and insulin resistance in humans.

The Cav1-PPARγ interaction site confers ligand sensitivity. To more carefully map the binding site between Cav1 and PPARγ, we created two deletions in PPARγ helix 7 (Fig. 5A) (ΔH7/1 aa 366 to 372 and ΔH7/2 aa 358 to 363), both of which remove the phenylalanine-rich stretch hypothesized to form the hydrophobic interface for binding of Cav1 (**F**GD**F**MEPK **FEF**; phenylalanines are in boldface). We also made the corresponding deletion in Cav1 to remove the sequence FTV TKYW in the CSD (ΔCSD aa 82 to 101), which mediates binding to canonical Cav1-interacting proteins (14).

Cotransfection of WT or mutant Cav1 and PPARγ expression plasmids into HEK293 cells followed by CoIP experiments demonstrated that the H7 and CSD mutants were incapable of interacting compared to WT proteins (Fig. 5A). We next asked

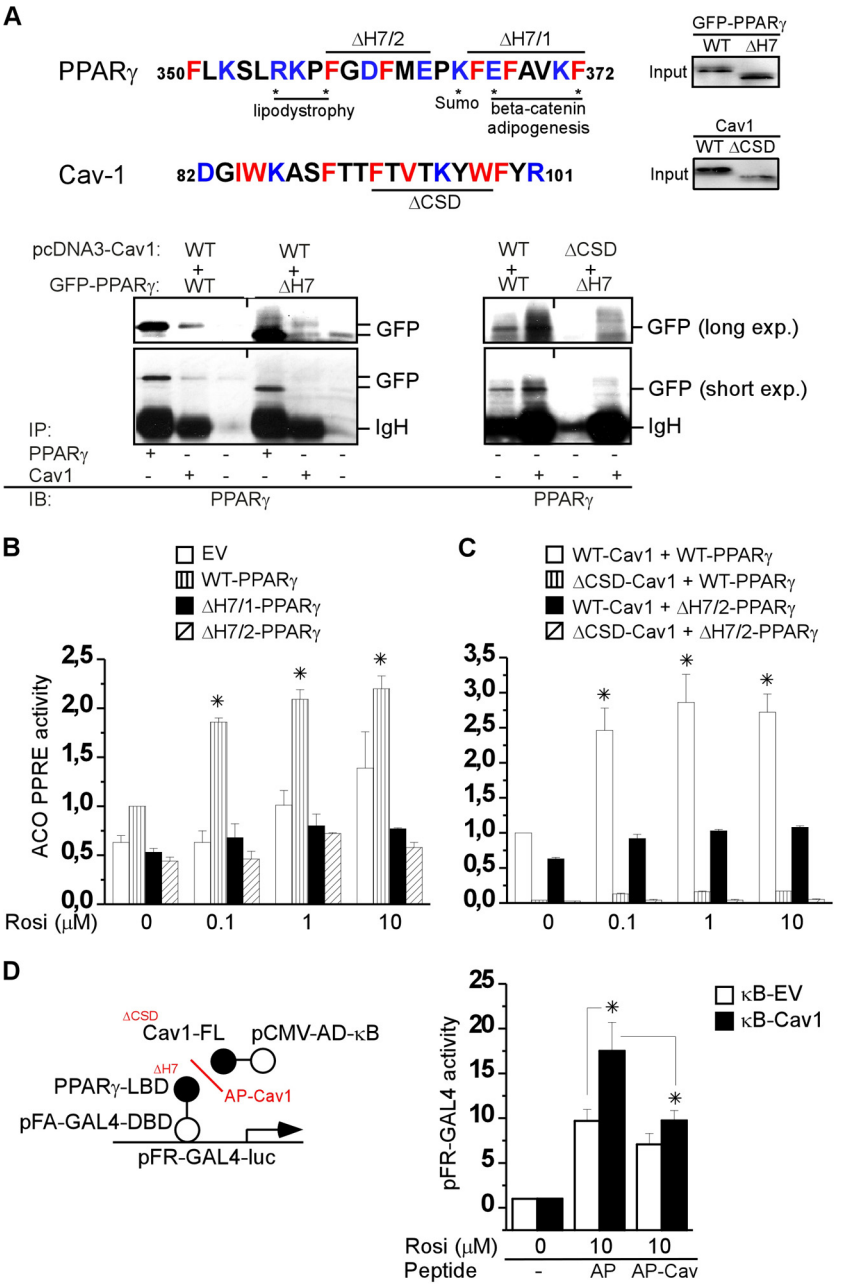

FIG. 5. Helix 7 in the LBD of PPARγ harbors a Cav1-binding motif. (A) Mapping of the PPARγ-Cav1 interaction site by CoIP. (Top) Human peptide sequences within the putative docking interfaces of helix 7 (H7) in the PPARγ LBD (aa 350 to 372) and the scaffolding domain (CSD) of Cav1 (aa 82 to 101). Red, aromatic/hydrophobic amino acids; blue, charged amino acids. (Lower) Deletion of helix 7 (ΔH7/2 and ΔH7/1) and the CSD (ΔCSD) abrogates interaction of PPARγ with Cav1. HEK293 cells were transiently cotransfected with WT or ΔH7 GFP-PPARγ together with WT or ΔCSD pcDNA3 plasmids. Representative WBs of inputs and CoIPs are presented. (B) Deletion of H7 renders PPARγ dominant negative. HEK293 cells were transiently cotransfected with the PPRE reporter plasmid, PPARγ constructs, or empty vector (EV) and were treated for 24 h with rosiglitazone. Luciferase values normalized to protein content are indicated as fold changes ± SE ($n = 3$) compared to the value for the vehicle control. *, $P < 0.05$ for WT versus mutants. (C) Deletion of H7 and the CSD abrogates ligand-dependent PPRE transcription. HEK293 cells were transfected as described for panel B, together with the WT or mutant Cav1 construct. *, $P < 0.05$ for WT versus mutants. (D) Cell-permeable peptides of the CSD disrupt the interaction of Cav1 and the PPARγ-LBD in a mammalian 2-hybrid experiment. HEK293 cells were transiently cotransfected with pFR-GAL4-UAS-luc reporter plasmid together with EV- or Cav1-NF-κB fusion constructs (prey) and the PPARγ-LBD-GAL4 bait vector for 24 h. Peptides (AP and AP-Cav1) and rosiglitazone were added for an additional 24 h. Luciferase values normalized to protein content are indicated as fold changes ± SE ($n = 3$) compared to values for vehicle-treated controls. *, $P < 0.05$ for EV(prey) versus Cav1(prey) or for AP control versus AP-Cav1 peptide.

whether loss of Cav1-PPARγ binding alters the transcriptional activity of PPARγ. WT and ΔH7 GFP-PPARγ constructs were cotransfected into HEK293 cells together with the PPRE reporter plasmid, and cells were treated for 24 h with 1 μM rosiglitazone. In contrast to WT GFP-PPARγ, the ΔH7/1 and ΔH7/2 mutants were ligand unresponsive and, moreover, inhibited endogenous PPARγ activity in a dominant-negative fashion (Fig. 5B). When WT or ΔH7 mutants of PPARγ were cotransfected with either WT or ΔCSD-Cav1, the ΔCSD was even more effective in repression of the ligand-mediated transactivation of the PPRE reporter than the ΔH7 mutants alone (Fig. 5C). These results corroborated that the interaction between PPARγ and Cav1 is required for ligand-dependent transcriptional activity of PPARγ.

To verify the Cav1-PPARγ interaction by an independent approach, we performed a mammalian 2-hybrid interaction experiment with HEK293 cells (Fig. 5D). Cells were transiently cotransfected with the reporter plasmid pFR-GAL4-UAS-luc, pFA-GAL4-PPARγ-LBD (bait), and pCMV-AD-κB (prey) vector harboring full-length Cav1. Cells were then incubated with rosiglitazone in the absence or presence of a cell-permeable CSD peptide mimic (AP-Cav1) or a control (AP) peptide for 24 h. Luciferase assays revealed that the association between the bait (PPARγ) and prey (Cav1-κB) proteins was increased by the ligand and was disrupted by the CSD peptide. TPA had no effect (data not shown). These data confirmed that Cav1 and PPARγ interact through their CSD and the LBD in a ligand-dependent fashion.

To visualize the subcellular localizations of PPARγ and Cav1, immunofluorescence microscopy was performed (see Fig. S5 at http://www.gastric.de/typo3_mannheim/index.php?id=down000). WT and ΔH7/1 GFP-PPARγ constructs were transiently transfected into AGS clones. In AGS/EV cells, both GFP-PPARγ constructs localized to the nucleus. In AGS/Cav1 cells, an additional cytosolic distribution of WT GFP-PPARγ was observed, which was abrogated in ΔH7/1-transfected cells. Cav1 also localized to the plasma membrane in AGS clones and in transiently transfected HEK293 cells. In contrast, the ΔCSD mutant did not show membrane binding but accumulated in vesicular structures in the cell periphery. Similar to ΔH7/1, the ΔH7/2 mutant also remained in the nucleus. These results indicated that helix 7 is required for the cytosolic distribution of PPARγ by interaction with Cav1.

Endogenous Cav1 promotes PPARγ ligand-dependent transcription and growth inhibition. We next explored the functional role of endogenous Cav1 in cell proliferation and PPARγ ligand sensitivity. We used MKN45 clones, in which endogenous Cav1 had been knocked down by stable transfection of short hairpin RNA (shRNA) (MKN45/RNAi) as a comparison to a control RNAi (MKN45/Cav1) line (9). Cells were incubated with rosiglitazone, and growth was measured by MTT assays. MKN45 clones (50% inhibitory concentration [IC_{50}] = 10 to 20 μM) were generally more sensitive to ligand-dependent growth inhibition than were AGS clones (IC_{50} = 40 to 50 μM), evident in dose response and in time course experiments (see Fig. S6 at http://www.gastric.de/typo3_mannheim/index.php?id=down000). Cav1 expression did not significantly alter the modest response of AGS cells to rosiglitazone, which may be due to the K-Ras mutation G12D, which, similar to G12V in SW480 cells (40), renders the GTPase constitutively active (63), leading to posttranslational inactivation of PPARγ.

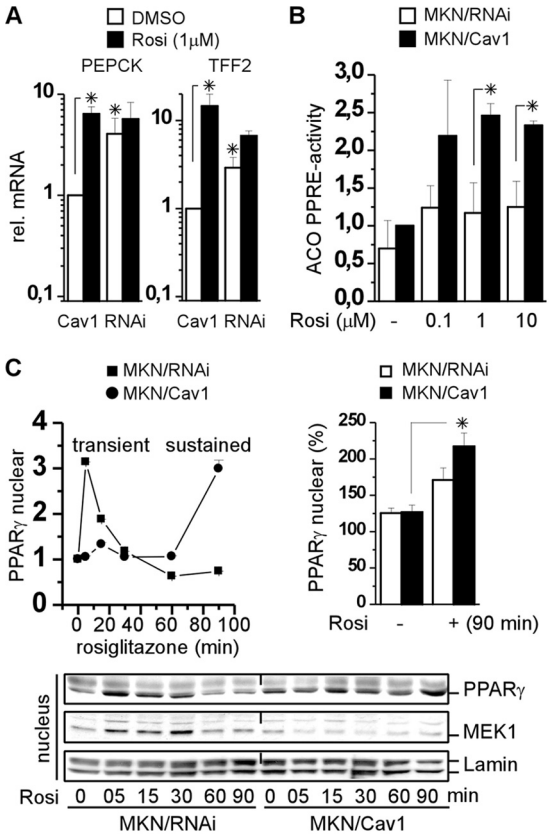

FIG. 6. Endogenous Cav1 promotes nuclear translocation and ligand-dependent transcription of PPARγ target genes. (A) mRNA expression. MKN45 clones were treated for 16 h with vehicle or 1 μM rosiglitazone. C_T values from RT-qPCRs were normalized to the value for β2-microglobulin and calculated as fold changes ± SE (n = 5 per clone). *, $P < 0.05$ for MKN45/Cav1 versus MKN45/RNAi or for MKN45/Cav1 ROSI versus DMSO. (B) Transactivation. MKN45 clones were transiently transfected with PPRE reporter and incubated for 24 h with rosiglitazone. Luciferase values normalized to protein content are indicated as fold changes ± SE (n = 3) relative to values for vehicle-treated controls. *, $P < 0.05$ for MKN45/Cav1 versus MKN45/RNAi. (C) Endogenous Cav1 facilitates sustained nuclear import of PPARγ. Serum-deprived MKN45 clones were treated with 10 μM rosiglitazone for the indicated times. Results for quantitative analyses (top panel) are displayed together with representative WBs (bottom panel). OD values from WB gels were normalized to the value for lamin A/C and calculated as percentages ± SE (n = 5) compared to values for vehicle controls. *, $P < 0.05$ for ROSI versus DMSO.

In contrast, MKN45 contains wild-type K-Ras G12 (unpublished observation), and MKN45/Cav1 cells were 2-fold more responsive to rosiglitazone than MKN45/RNAi cells, indicating that endogenous Cav1 augments the antiproliferative response of cells to PPARγ ligands.

Similar to AGS/EV cells, MKN45/RNAi cells formed an increased number of MEK1-PPARγ complexes (data not shown), showed reduced cytosolic retention of PPARγ (see Fig. S5 at http://www.gastric.de/typo3_mannheim/index.php?id=down000), and showed an exaggerated ligand-independent transcription of PPARγ target genes (Fig. 6A) compared to MKN45/Cav1 cells. Together, these observations point at a common cellular mechanism of Cav1-mediated cytosolic sequestration of PPARγ. In contrast to AGS/Cav1 cells, MKN45/Cav1 cells showed enhanced

activation of PPARγ target genes (Fig. 6A) and the PPRE reporter (Fig. 6B) in response to rosiglitazone compared to MKN45/RNAi clones. Similar results were obtained from transiently transfected parental MKN45 and N87 cells (not shown). To explore the basis for this cell-type-specific response, subcellular fractionation studies were performed as previously done with AGS clones. In MKN45/Cav1 cells, a sustained import of PPARγ into the nucleus was observed upon a 90-min incubation with rosiglitazone (Fig. 6C). In contrast, PPARγ and MEK1 rapidly (5 min) accumulated in the nuclei of MKN45/RNAi cells, reached a transient maximum (15 to 30 min), and then became undetectable (60 to 90 min). TPA evoked a similar relocalization response (data not shown). Thus, endogenous Cav1 in MKN45 cells promotes sustained nuclear translocation of PPARγ, preserving response to rosiglitazone, an effect not present in AGS/Cav1 cells, due to cytosolic sequestration of PPARγ.

Dok1 cooperates with endogenous Cav1 as a ligand sensitizer for PPARγ. To understand the apparent cell-specific effects of Cav1 in regulation of PPARγ activity, we immunoprecipitated Cav1 from whole-cell lysates of parental MKN45 cells and identified associated proteins. MALDI-MS identified an ~36-kDa protein to contain peptides of human docking protein (Dok1) (see Table S3 at http://www.gastric.de/typo3_mannheim/index.php?id=down000). At least three variants of human Dok1 have been described (25, 29, 37) (Fig. 7A). The p62 full-length Dok1 isoform 1 has pleckstrin homology (PH) and protein tyrosine binding (PTB) domains. The small C-terminally truncated p19-p22 isoform 2 variant misses the PTB and the C-terminal two-thirds of the protein, while an N-terminally truncated p37-p44 isoform 3 variant lacks the PH domain. In AGS cells, only the isoform p37-p44 isoform (29) was detectable, while in MKN45 cells all three variants were present (Fig. 7B). CoIP using a Dok1-specific antibody (24) confirmed the precipitation of p37-p44 Dok1 by Cav1 in MKN45 but not in AGS cells (data not shown). Dok1 is an adaptor protein that interferes with receptor tyrosine kinase signaling, e.g., in the epidermal growth factor (EGF)-human epidermal growth factor receptor (HER)-Ras-MAPK pathway (37). Dok1 promotes PPARγ activity by inhibition of ERK1/2-mediated S82 phosphorylation *in vivo* (24).

To test whether Dok1 isoforms cooperate with Cav1 as ligand sensitizer for PPARγ, Dok1 expression in whole-cell lysates of parental GC lines was determined by WB (Fig. 7C), and its effect on ligand sensitivity was examined by MTT proliferation and reporter gene assays. Cell lines derived from primary GC (AGS and SNU1) generally had low Dok1 levels and were less responsive to ligand-mediated transactivation (Fig. 7C) and growth inhibition (Fig. 7D) than cell lines with high-level Dok1 expression (MKN45, N87, and MKN7). Immunofluorescence microscopy detected Dok1 enriched on the plasma membrane in MKN45 cells. In contrast, Dok1 was diffusely distributed in the cytoplasm of AGS cells (Fig. 8A). Both rosiglitazone and TPA triggered a robust translocation of PPARγ into the nucleus within 60 min in MKN45 cells but not in AGS cells. Dok1 may thus enhance the sensitivity of cells to PPARγ activation by promoting its nuclear translocation. Indeed, silencing of endogenous Dok1 in MKN45 cells by transient transfection of siRNA reduced ligand-mediated activation of the (ACO) PPRE reporter (Fig. 8B). Dok1 knockdown also increased the resistance of parental AGS and SW480 cells toward rosiglitazone-mediated growth inhibition (data not shown). *Vice versa*, overexpression of human full-length p62 Dok1 in MKN45 cells enhanced ligand-dependent PPRE reporter activation compared to the level in cells transfected with control vector (Fig. 8C). Similar results were obtained with SW480 cells (not shown). Collectively, these data suggest that Cav1, in cooperation with Dok1, increases the ligand-dependent transcriptional activity of PPARγ.

Activation of PPARγ upregulates *dok1* and inhibits proliferation in a mouse model of GC. To explore the role of PPARγ in GC cell proliferation *in vivo*, transgenic CEA424-SV40 T-antigen (Tag) mice (59) were fed a chow diet enriched with 0,02% (wt/wt) rosiglitazone (~25 mg/kg/day) (30). Tag mice express the SV40 T-antigen under the control of the human carcinoembryonic antigen (CEA) promoter, leading to a highly proliferative intraepithelial carcinoma in the pylorus region of the stomach (Fig. 9A). The gastric tumor appears with full penetrance at an age of 30 days, and mice are moribund at about 3 months of age. Tag mice had reduced gastric levels of PPARγ, Cav1, and Dok1 mRNA and protein compared to pyloric tissue from C57BL/6N wild-type littermates (see Fig. S7 at http://www.gastric.de/typo3_mannheim/index.php?id=down000), consistent with a loss of Ras/MAPK-inhibitory proteins in the tumor. Rosiglitazone was fed to 4-week-old Tag mice for additional 6 weeks, along with a control group that received standard chow ($n = 5$ per group). The frequencies of Ki-67 (Fig. 9B)- and BrdU (not shown)-positive cells were significantly reduced within the tumor areas in the rosiglitazone-fed animals compared to the level for the control. The mRNAs of PPARγ-regulated genes (*tff1*, *aco*, and *pepck*) were significantly upregulated by rosiglitazone (see Fig. S7 at the URL mentioned above), and interestingly, rosiglitazone-treated animals also had higher levels of *cav1*, *pparγ*, and *dok1* mRNA (Fig. 9C). This finding confirmed previous studies (8, 10, 35) that showed that Cav1 is downregulated in human primary GC and that PPARγ transcriptionally upregulates Cav1 gene expression *in vitro*.

Together, these data demonstrate that PPARγ activation inhibits growth of human and murine GC cells both *in vitro* and *in vivo*, and its responsiveness to ligands is amplified by the presence of the Ras/MAPK inhibitors Cav1 and Dok1.

DISCUSSION

Our results support a novel molecular mechanism for spatial regulation of PPARγ signaling through subcellular compartmentalization in gastric cancer (GC) cells. We have shown that two PPARγ partner proteins, by binding to distinct docking surfaces on its ligand-binding domain (LBD), Cav1 at helix 7 and MEK1 at helix 12, alter PPARγ's subcellular localization and activity (Fig. 10).

How is this regulation achieved? Constitutive activation of the EGF receptor (EGFR)/HER-Ras-Raf-MEK1/2-ERK1/2 cascade is a frequent event in human cancers. ERK1/2 promote cyclin D1 synthesis and proliferation. Active MEK1 and ERK1/2 move from the cytosol to the nucleus via a recently identified nuclear translocation signal (NTS/SPS) (12) in their kinase domains. While no classical nuclear localization signal (NLS) has been characterized in PPARγ, we showed previously that MEK1 interacts with PPARγ upon stimulation with either mitogen or ligand (4), evoking rapid export of PPARγ

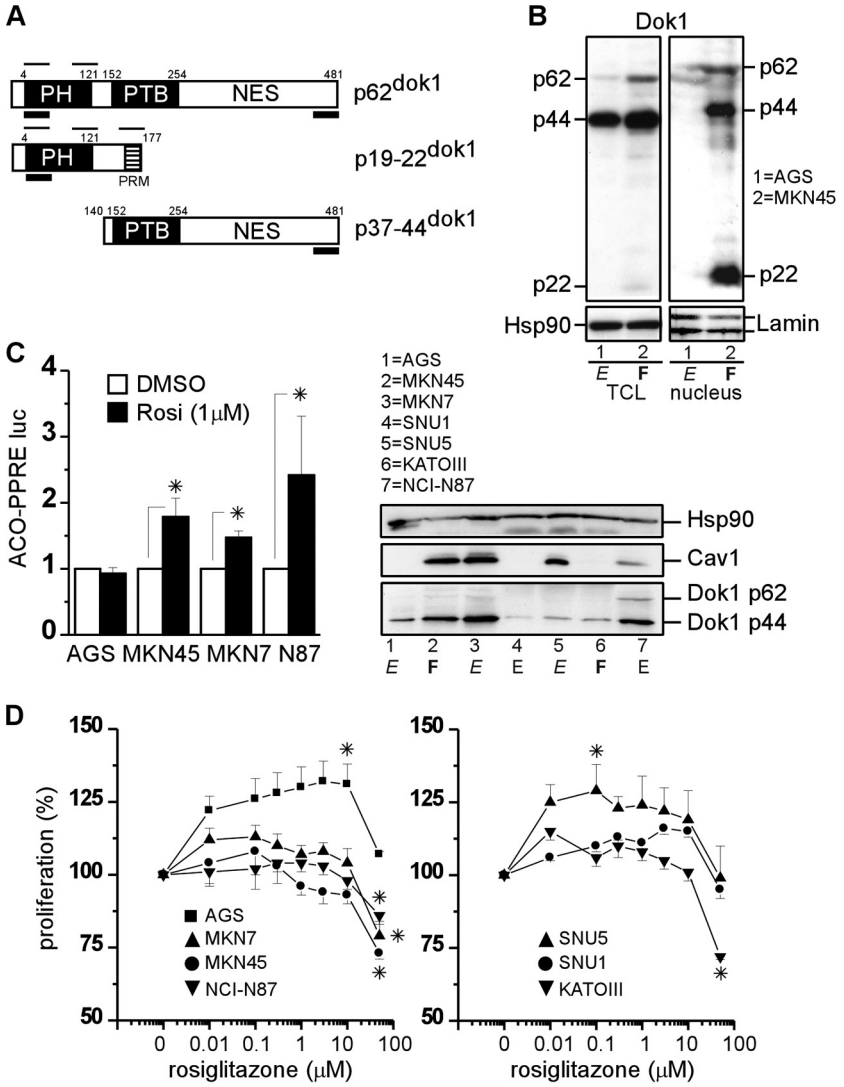

FIG. 7. Dok1 cooperates with endogenous Cav1 to inhibit cell growth. (A) Dok1 splice/translational variants in human cancer cells. PH, pleckstrin homology domain; PTB, protein tyrosine binding domain; NES, nuclear export sequence (alike in MEK1). Bold bars, variant-selective RT-PCR amplicons; line bars, MALDI peptides. (B) WBs detecting Dok1 protein variants in total cell lysates (TCL) (left panel) and nuclear extracts (right panel) of parental GC lines. (C) Correlation of Dok1 expression in parental GC cell lines to transcriptional activation by PPARγ ligand. (Left) Cells were transiently cotransfected with the PPRE reporter and incubated for 24 h with 1 μM rosiglitazone. Firefly luciferase values were normalized to *Renilla* luciferase counts and are indicated as fold changes ± SE ($n = 3$) compared to values for vehicle-treated controls. *, $P < 0.05$ for ROSI versus DMSO. (Right) Representative WBs detecting the predominant Dok1 p44 isoform 3 and p62 isoform 1. (D) Dok1 expression relates to enhanced sensitivity to PPARγ ligand-mediated growth inhibition. Parental GC cell lines were incubated with increasing concentrations of rosiglitazone for 4 days. OD values from MTT assays were calculated as percentages ± SE ($n = 3$). *, $P < 0.05$ for ROSI versus DMSO.

out of the nucleus. This phenomenon requires the nuclear export sequence (NES) on MEK1. These data suggest that MEK1 acts as a mobile and reversible cytoplasmic-nuclear shuttle for PPARγ. In addition, PPARγ is subjected to phosphorylation through ERKs at serine 84 (serine 82 in mice) (60), which antagonizes its ligand-dependent transcriptional activity. In Cav1-deficient AGS/EV and MKN45/RNAi cells, we observed an increased intercompartmental mobility of serine 84-phosphorylated PPARγ in complex with MEK1. We conclude that MEK1 promotes rapid nuclear translocation of PPARγ to support basal, ligand-independent transcription of PPARγ target genes (such as the TFF2 gene) and cyclin D1. In the absence of Cav1, active MEK/ERK signaling thus accelerates cell division.

Vice versa, Cav1 decreased proliferation by inhibition of cyclin D1 gene transcription at the G_1/S phase of the cell cycle. In AGS/Cav1 cells, the PPARγ ligand rosiglitazone promoted the association of PPARγ with both Cav1 and MEK1 in the cytosol. How can this trimolecular complex repress cyclin D1 activity? Cav1 has been shown to inhibit proliferation by sequestration of the upstream MAPK cascade proteins, including Ras, Raf, MEK1, and growth factor receptors in membrane caveolae, and by direct interaction via its scaffolding domain (CSD) (14). The binding of MEK1 by Cav1 and PPARγ in the

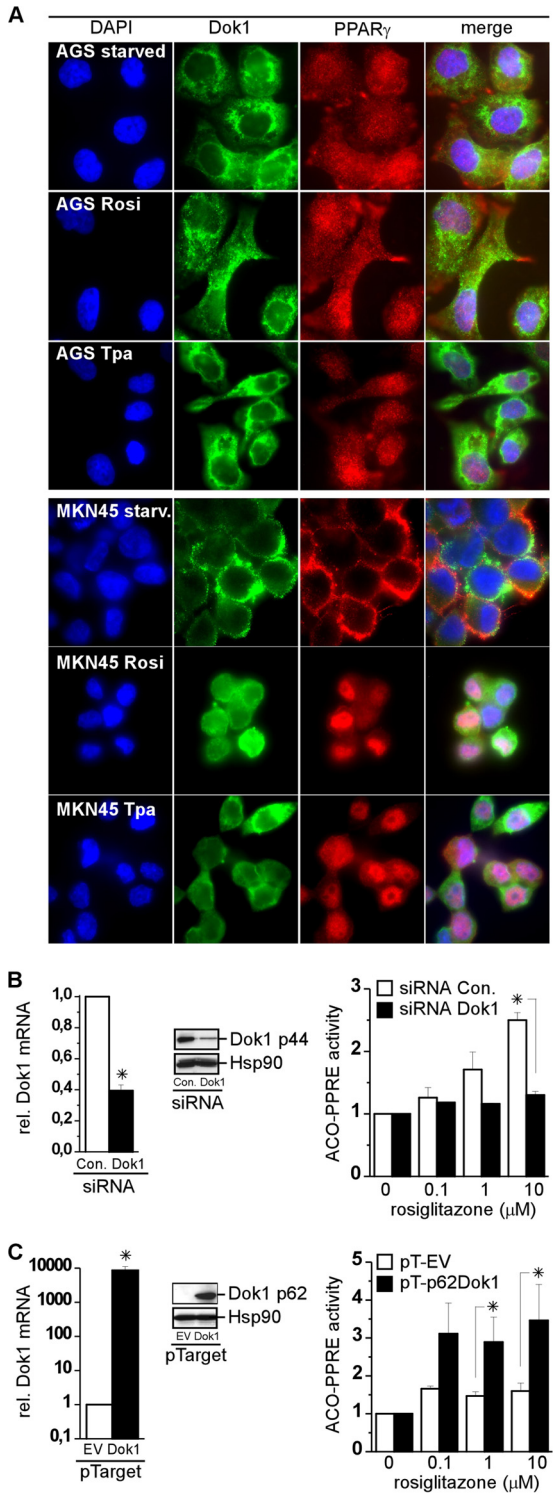

FIG. 8. Dok1 augments the ligand-dependent transcriptional activity of PPARγ. (A) Immunofluorescence microscopy of Dok1 showing nuclear translocation of endogenous PPARγ in MKN45 cells but not in AGS cells. Parental GC cells were deprived of serum and stimulated for 60 min with rosiglitazone (10 μM) or TPA (100 nM). Green, Dok1; red, PPARγ; blue, nuclei. Magnification, ×630. (B) Knockdown of endogenous Dok1 by siRNA reduces the ligand-dependent transcriptional activity of PPARγ in MKN45 cells. (Left) Validation of Dok1 silencing by RT-qPCR (detecting all 3 Dok1 isoforms) and WB. (Right) Cells were cotransfected with the PPRE reporter and treated for 24 h with 1 μM rosiglitazone. Firefly luciferase values were normalized to *Renilla* luciferase counts and are indicated as fold changes ± SE ($n = 3$) compared to values for vehicle-treated controls. ∗, $P < 0.05$ for Dok1 siRNA versus control siRNA. (C) Overexpression of human p62 Dok1 enhances ligand-dependent PPARγ transcriptional activity. (Left) Validation of transfected full-length p62 Dok1 in HEK293 cells by RT-qPCR and WB. (Right) MKN45 cells were transfected and treated as described for panel B.

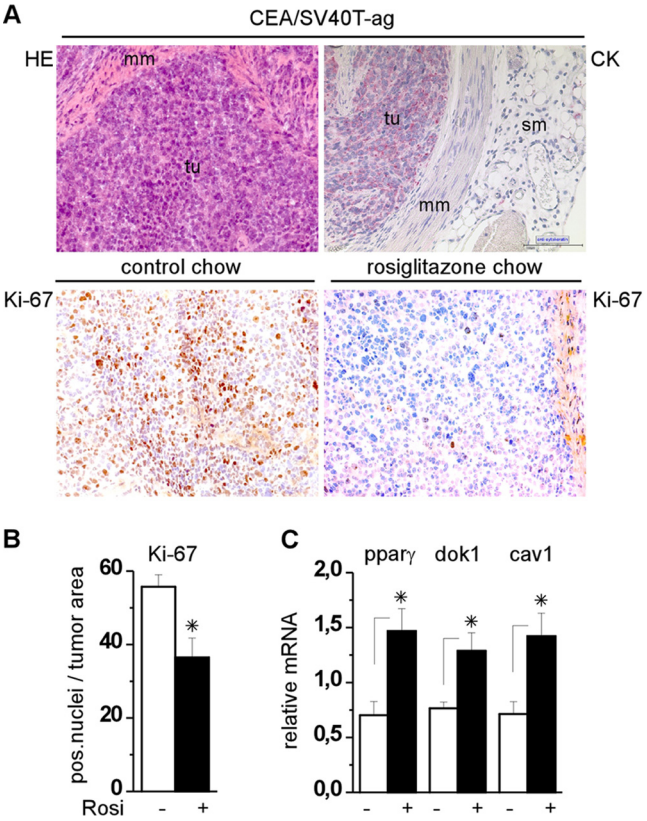

FIG. 9. PPARγ activation inhibits proliferation and upregulates *Dok1* in a murine model of GC. (A) Reduced proliferation in pyloric tumor areas of stomachs from CEA424-SV40 T-antigen (Tag) mice upon a 6-week chow diet enriched with 0.02% (wt/wt) rosiglitazone compared to the level for the control diet ($n = 5$ per group). (Top) H&E staining and IHC against Pan-CK (red), marking the epithelial nature of the tumor. (Bottom) Representative IHC for Ki-67 (brown) is presented above the results for the quantitative analysis represented in panel B. Magnifications, ×100 and ×200. (B) Numbers of Ki-67-positive nuclei per tumor field ($n = 5$ fields) were counted. ∗, $P < 0.05$ for chow versus ROSI. (C) Upregulation of gastric mRNAs in Tag mice by rosiglitazone. C_T values from RT-qPCRs normalized to the value for β2-microglobulin were calculated as fold changes ± SE ($n = 5$ per genotype). ∗, $P < 0.05$ for chow versus ROSI.

cytosol may lead to the inactivation of its kinase activity and reduced downstream signaling of MEK1 toward the cell cycle machinery. Cyclin D1 is not directly regulated by PPARγ. Instead, PPARγ inhibits cyclin D1 synthesis and upregulates CDK inhibitors indirectly via other transcription factors (C/EBP, CREB, and APC/β-catenin), which participate in differentiation of epithelial and mesenchymal cells (20, 55, 65). Mutation of the Cav1 interaction site in helix 7 of PPARγ

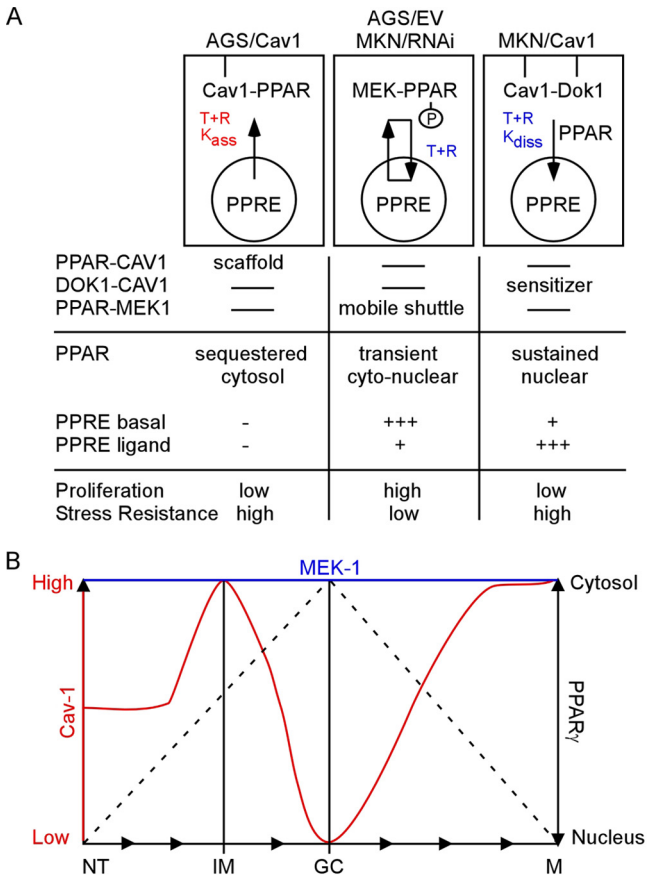

FIG. 10. Model of PPARγ interactions with Ras/MAPK inhibitors in human GC. (A) Cav1 in (K-Ras mutated) AGS cells acts as a sequestor for PPARγ, inhibiting basal and ligand-dependent transcription of PPARγ target genes. Loss of Cav1 leads to pronounced binding of PPARγ to MEK1 and its phosphorylation by ERK1/2, promoting transient cyto-nuclear shuttling and basal transcription of PPARγ target genes (PPRE) and cyclin D1. Cav1 in (K-Ras wild-type) MKN45 cells cooperates with Dok1 to promote sustained accumulation of PPARγ in the nucleus, enhancing ligand-dependent activation of PPARγ target genes. Loss of Cav1 facilitates MEK/ERK-mediated inhibition of PPARγ and stimulates proliferation, while Cav1 in conjunction with Dok1 prevents activation of the Ras/MAPK cascade and posttranslational inactivation of PPARγ, resulting in reduction of cell growth. Circle, nucleus; square, plasma membrane; $K_{ass/diss}$, mitogen (TPA; T) and ligand (rosiglitazone; R) promote dynamic dissociation/association cycles of PPARγ from/to partner proteins. (B) PPARγ compartmentalization in human GC tissue. Lower *x* axis, time of initiation and progression of human GC; NT, normal; IM, intestinal metaplasia; GC, (intestinal-type) gastric cancer; M, (metastatic) gastric cancer; left *y* axis, Cav1 expression levels (red line); right *y* axis, PPARγ cytoplasmic-to-nuclear distribution (black dotted line); upper *x* axis, cytosolic MEK1 (blue line). In the normal stomach, PPARγ resides in the nucleus and Cav1 in the cytosol to maintain tissue differentiation. In intestinal metaplasia (IM), cytosolic Cav1 expression is increased and PPARγ is inactivated by its relocalization to the cytoplasm, where it is likely to encounter MEK1. In GC, Cav1 expression is lost and PPARγ moves back to the nucleus proportional to the degree of tumor dedifferentiation. Regain of Cav1 and nuclear PPARγ in an advanced stage of GC may provide survival benefit for tumor cells through pronounced activation of noncanonical target genes (such as the TFF2 gene).

increased cell proliferation (unpublished observation). In humans, mutations, both in helix 7 of PPARγ (1, 22, 34, 47, 64) and in components of caveolae, are associated with lipodystrophy (48, 57). Moreover, Cav1-KO mice have metabolic defects and abnormalities in lipid storage (49). Both the human and the mouse phenotypes share an underlying defect in adipose differentiation, where PPARγ is a master player. This similarity in phenotype, based on genetic evidence, supports our data demonstrating direct mechanistic cooperation of Cav1 and PPARγ in control of cell growth and differentiation. Future studies will be needed to clarify the molecular mechanisms linking regulation of the Cav1-PPARγ complex to the cell cycle machinery.

We were initially surprised by an apparent paradox when we observed that endogenous Cav1 promoted ligand-dependent PPARγ activity in MKN45/Cav1 cells while inhibiting it through cytosolic sequestration of PPARγ in AGS/Cav1 cells. How could Cav1 simultaneously enhance the ligand sensitivity of PPARγ while reducing its basal transcriptional activity? Cav1 functions as a scaffold protein controlling the activity of partner molecules, but it also directly binds cholesterol and lipids. The conserved Cav1-binding motif that we identified in helix 7 of PPARγ was also conserved in other NRs that regulate genes in lipid/cholesterol metabolism (PPARα/δ, FXR, LXR, and CAR) (see Table S2 at http://www.gastric.de/typo3_mannheim/index.php?id=down000). It is interesting to speculate that, because of its dual role as a scaffold and cholesterol/lipid binding protein, Cav1 may bind to NRs directly, leading to their spatial immobilization, and also promote ligand transfer through close contact. In such a model, Cav1 would facilitate the transport of hydrophobic natural ligands (e.g., fatty acids, sterols, and 15d-PGJ_2) via the plasma membrane to PPARγ or other NRs through vesicular endocytotic mechanisms ("caveosomes") (46) or in cooperation with cytosolic lipid binding proteins (such as fatty acid binding proteins [FABPs]) (58). We have previously detected Cav1-bound PPARγ in human colon adenocarcinoma HT29 and HCT116 cells, where PPARγ increased expression of Cav1 and villin, a differentiation marker of the intestine (8). Others have reported relocalization of PPARγ in macrophages (61, 62) and in adipocytes (27, 51) in response to extracellular stimuli, supporting cooperation of Cav1 and PPARγ in the regulation of metabolism and cell differentiation in other cell types. These data, together with studies on steroid hormone receptors (38, 54), point at a more general principle of Cav1-mediated regulation of NR function.

The identification of the signaling adapter and endogenous Ras/MAPK inhibitor Dok1 provided a mechanistic explanation for the dual role of Cav1 as a scaffold sequestor and a ligand sensitizer. Dok1 shuttles between the plasma membrane and the nucleus in response to mitogens (43), similar to MEK1, by means of a functional NES. When Dok1 is present, it may facilitate release of PPARγ from its sequestering proteins MEK1 and Cav1 and, upon binding to ligand, promote its nuclear translocation. The role of Dok1 in inhibiting the Ras/MAPK cascade as well as in preventing the ERK1/2-mediated phosphorylation of PPARγ at S84 (S82 in mice) (24) suggests that these two events may synergize to promote PPARγ activity. Accordingly, we found that cells with high Dok1 and wild-type K-Ras were ligand responsive (MKN45, MKN7, N87, and

HCT116). Downregulation of Dok1 expression in tissues (unpublished observation) and cell lines (AGS and SNU1) derived from primary GC has been reported by us and for lung cancer (3). K-Ras mutations may underlie therapy failure in human colorectal cancer patients (26). Thus, the lack of Cav1 and Dok1, combined with a constitutive active K-Ras mutation, as in AGS, SNU1, and SW480 cells, may account for enhanced serine 84 phosphorylation of PPARγ and resistance to ligand-mediated growth inhibition in these human cancer cells (40, 63).

Our data also indicate that Cav1 regulates PPARγ localization *in vivo* (Fig. 10). In the normal human gastric mucosa, Cav1 localizes to the cytosol of gastric gland epithelial cells (9), while PPARγ resides in the nucleus (45). In intestinal metaplasia (IM), a putative preneoplastic lesion of GC, cytosolic Cav1 was increased, and PPARγ was redistributed to the cytosol, indicative of an association of the two molecules *in vivo*. In contrast, Cav1 was downregulated in murine GC tissue, consistent with previous reports on human primary GC (2, 9) and confirming that loss of Cav1 is a hallmark of mitotic cells (33, 50). Consistent with the putative roles of Cav1 and PPARγ as tumor suppressors, our *in vivo* studies confirmed that the presence of Cav1 and the activation of PPARγ decreased cell proliferation in the nonneoplastic stomach and in GC in mice. PPARγ promoted Cav1 mRNA expression (8), and Cav1, together with Dok1, enhanced ligand-dependent transactivation by PPARγ, suggesting a positive amplification loop between the two molecules. Notably, expression of Cav1 and nuclear PPARγ is reactivated in tissues from patients with advanced GC and in human GC cells from distant metastases (MKN45, KATOIII, and SNU5) (9, 45). In addition to its growth-inhibitory role, Cav1 renders GC cells more resistant to stress (9). Thus, a positive selection pressure for PPARγ to activate target genes (such as the TFF2 gene) involved in cell survival may predominate in advanced cancer stages.

Since the EGFR/HER family of receptor tyrosine kinases has been associated with GC progression and patient survival (as reviewed in reference 41), combination therapy of GC targeting PPARγ and kinases together may be envisioned in the future. However, novel approaches must involve consideration that PPARγ acts in a stage- and tissue-dependent manner, due to its multiple interactions with regulatory proteins in diverse cell compartments, which determine its overall effect on target gene regulation and signaling networks.

ACKNOWLEDGMENTS

In memory of Mordechai Liscovitch, we are indebted to his profound advice, support, and mentorship. We thank Duarte Afonso for technical help and Hans-Peter Märki for supply of ligands.

This study was supported by grants to E.B. and M.P.A.E. from the Deutsche Krebshilfe (108287) and DFG (BU-2285). M.P.A.E. is also supported by grants from the Deutsche Krebshilfe (107885), DFG (SFB 824, TP B1), Else Kröner Stiftung (no. P14/07//A104/06), and BMBF (Mobimed 01EZ0802; KMU-innovativ no. 0315116B). We have no conflicts of interest to disclose.

REFERENCES

1. **Agostini, M., et al.** 2004. Tyrosine agonists reverse the molecular defects associated with dominant-negative mutations in human peroxisome proliferator-activated receptor gamma. Endocrinology **145:**1527–1538.
2. **Barresi, V., G. Giuffre, E. Vitarelli, P. Todaro, and G. Tuccari.** 2008. Caveolin-1 immuno-expression in human gastric cancer: histopathogenetic hypotheses. Virchows Arch. **453:**571–578.
3. **Berger, A. H., et al.** 2010. Identification of DOK genes as lung tumor suppressors. Nat. Genet. **42:**216–223.
4. **Burgermeister, E., et al.** 2007. Interaction with MEK causes nuclear export and downregulation of peroxisome proliferator-activated receptor gamma. Mol. Cell. Biol. **27:**803–817.
5. **Burgermeister, E., et al.** 2006. A novel partial agonist of peroxisome proliferator-activated receptor-gamma (PPARgamma) recruits PPARgamma-coactivator-1alpha, prevents triglyceride accumulation, and potentiates insulin signaling in vitro. Mol. Endocrinol. **20:**809–830.
6. **Burgermeister, E., and R. Seger.** 2007. MAPK kinases as nucleo-cytoplasmic shuttles for PPARgamma. Cell Cycle **6:**1539–1548.
7. **Burgermeister, E., and R. Seger.** 2008. PPARgamma and MEK Interactions in Cancer. PPAR Res. **2008:**309469.
8. **Burgermeister, E., L. Tencer, and M. Liscovitch.** 2003. Peroxisome proliferator-activated receptor-gamma upregulates caveolin-1 and caveolin-2 expression in human carcinoma cells. Oncogene **22:**3888–3900.
9. **Burgermeister, E., et al.** 2007. Differential expression and function of caveolin-1 in human gastric cancer progression. Cancer Res. **67:**8519–8526.
10. **Chen, X., et al.** 2010. Integrin alpha1beta1 regulates epidermal growth factor receptor activation by controlling peroxisome proliferator-activated receptor gamma-dependent caveolin-1 expression. Mol. Cell. Biol. **30:**3048–3058.
11. **Choi, J. H., et al.** 2010. Anti-diabetic drugs inhibit obesity-linked phosphorylation of PPARgamma by Cdk5. Nature **466:**451–456.
12. **Chuderland, D., A. Konson, and R. Seger.** 2008. Identification and characterization of a general nuclear translocation signal in signaling proteins. Mol. Cell **31:**850–861.
13. **Couet, J., S. Li, T. Okamoto, T. Ikezu, and M. P. Lisanti.** 1997. Identification of peptide and protein ligands for the caveolin-scaffolding domain. Implications for the interaction of caveolin with caveolae-associated proteins. J. Biol. Chem. **272:**6525–6533.
14. **Couet, J., M. Sargiacomo, and M. P. Lisanti.** 1997. Interaction of a receptor tyrosine kinase, EGF-R, with caveolins. Caveolin binding negatively regulates tyrosine and serine/threonine kinase activities. J. Biol. Chem. **272:** 30429–30438.
15. **Demers, A., et al.** 2009. A concerted kinase interplay identifies PPARgamma as a molecular target of ghrelin signaling in macrophages. PLoS One **4:**e7728.
16. **Ebert, M. P., et al.** 2006. Identification and confirmation of increased fibrinopeptide a serum protein levels in gastric cancer sera by magnet bead assisted MALDI-TOF mass spectrometry. J. Proteome Res. **5:**2152–2158.
17. **Gampe, R. T., Jr., et al.** 2000. Asymmetry in the PPARgamma/RXRalpha crystal structure reveals the molecular basis of heterodimerization among nuclear receptors. Mol. Cell **5:**545–555.
18. **Gratton, J. P., et al.** 2003. Selective inhibition of tumor microvascular permeability by cavtratin blocks tumor progression in mice. Cancer Cell **4:**31–39.
19. **Gupta, R. A., et al.** 2001. Activation of peroxisome proliferator-activated receptor gamma suppresses nuclear factor kappa B-mediated apoptosis induced by Helicobacter pylori in gastric epithelial cells. J. Biol. Chem. **276:** 31059–31066.
20. **Han, S., N. Sidell, P. B. Fisher, and J. Roman.** 2004. Up-regulation of p21 gene expression by peroxisome proliferator-activated receptor gamma in human lung carcinoma cells. Clin. Cancer Res. **10:**1911–1919.
21. **He, Q., J. Chen, H. L. Lin, P. J. Hu, and M. H. Chen.** 2007. Expression of peroxisome proliferator-activated receptor gamma, E-cadherin and matrix metalloproteinases-2 in gastric carcinoma and lymph node metastases. Chin. Med. J. (Engl.). **120:**1498–1504.
22. **Hegele, R. A., H. Cao, C. Frankowski, S. T. Mathews, and T. Leff.** 2002. PPARG F388L, a transactivation-deficient mutant, in familial partial lipodystrophy. Diabetes **51:**3586–3590.
23. **Holt, J. A., et al.** 2003. Helix 1/8 interactions influence the activity of nuclear receptor ligand-binding domains. Mol. Endocrinol. **17:**1704–1714.
24. **Hosooka, T., et al.** 2008. Dok1 mediates high-fat diet-induced adipocyte hypertrophy and obesity through modulation of PPAR-gamma phosphorylation. Nat. Med. **14:**188–193.
25. **Hubert, P., V. Ferreira, P. Debre, and G. Bismuth.** 2000. Molecular cloning of a truncated p62Dok1 isoform, p22Dok(del). Eur. J. Immunogenet. **27:** 145–148.
26. **Karapetis, C. S., et al.** 2008. K-ras mutations and benefit from cetuximab in advanced colorectal cancer. N. Engl. J. Med. **359:**1757–1765.
27. **Kawai, M., et al.** 2010. A circadian-regulated gene, Nocturnin, promotes adipogenesis by stimulating PPAR-gamma nuclear translocation. Proc. Natl. Acad. Sci. U. S. A. **107:**10508–10513.
28. **Kelly, D., et al.** 2004. Commensal anaerobic gut bacteria attenuate inflammation by regulating nuclear-cytoplasmic shuttling of PPAR-gamma and RelA. Nat. Immunol. **5:**104–112.
29. **Kobayashi, R., R. Patenia, S. Ashizawa, and J. Vykoukal.** 2009. Targeted mass spectrometric analysis of N-terminally truncated isoforms generated via alternative translation initiation. FEBS Lett. **583:**2441–2445.
30. **Lefebvre, A. M., et al.** 1998. Activation of the peroxisome proliferator-activated receptor gamma promotes the development of colon tumors in C57BL/6J-APCMin/+ mice. Nat. Med. **4:**1053–1057.

31. **Lehrke, M., and M. A. Lazar.** 2005. The many faces of PPARgamma. Cell **123:**993–999.
32. **Leung, W. K., et al.** 2004. Effect of peroxisome proliferator activated receptor gamma ligands on growth and gene expression profiles of gastric cancer cells. Gut **53:**331–338.
33. **Li, J., et al.** 2005. Loss of caveolin-1 causes the hyper-proliferation of intestinal crypt stem cells, with increased sensitivity to whole body gamma-radiation. Cell Cycle **4:**1817–1825.
34. **Liu, J., H. Wang, Y. Zuo, and S. R. Farmer.** 2006. Functional interaction between peroxisome proliferator-activated receptor gamma and beta-catenin. Mol. Cell. Biol. **26:**5827–5837.
35. **Llaverias, G., et al.** 2004. Rosiglitazone upregulates caveolin-1 expression in THP-1 cells through a PPAR-dependent mechanism. J. Lipid Res. **45:**2015–2024.
36. **Lu, J., et al.** 2005. Chemopreventive effect of peroxisome proliferator-activated receptor gamma on gastric carcinogenesis in mice. Cancer Res. **65:** 4769–4774.
37. **Mashima, R., Y. Hishida, T. Tezuka, and Y. Yamanashi.** 2009. The roles of Dok family adapters in immunoreceptor signaling. Immunol. Rev. **232:**273–285.
38. **Matthews, L., et al.** 2008. Caveolin mediates rapid glucocorticoid effects and couples glucocorticoid action to the antiproliferative program. Mol. Endocrinol. **22:**1320–1330.
39. **McAlpine, C. A., Y. Barak, I. Matise, and R. T. Cormier.** 2006. Intestinal-specific PPARgamma deficiency enhances tumorigenesis in ApcMin/+ mice. Int. J. Cancer **119:**2339–2346.
40. **McCoy, M. S., C. I. Bargmann, and R. A. Weinberg.** 1984. Human colon carcinoma Ki-ras2 oncogene and its corresponding proto-oncogene. Mol. Cell. Biol. **4:**1577–1582.
41. **Meza-Junco, J., H. J. Au, and M. B. Sawyer.** 2009. Trastuzumab for gastric cancer. Expert Opin. Biol. Ther. **9:**1543–1551.
42. **Nakajima, A., et al.** 2001. Endogenous PPAR gamma mediates anti-inflammatory activity in murine ischemia-reperfusion injury. Gastroenterology **120:** 460–469.
43. **Niu, Y., et al.** 2006. A nuclear export signal and phosphorylation regulate Dok1 subcellular localization and functions. Mol. Cell. Biol. **26:**4288–4301.
44. **Nolte, R. T., et al.** 1998. Ligand binding and co-activator assembly of the peroxisome proliferator-activated receptor-gamma. Nature **395:**137–143.
45. **Nomura, S., et al.** 2006. Differential expression of peroxisome proliferator-activated receptor in histologically different human gastric cancer tissues. J. Exp. Clin. Cancer Res. **25:**443–448.
46. **Parton, R. G., and K. Simons.** 2007. The multiple faces of caveolae. Nat. Rev. Mol. Cell Biol. **8:**185–194.
47. **Pascual, G., et al.** 2005. A SUMOylation-dependent pathway mediates transrepression of inflammatory response genes by PPAR-gamma. Nature **437:** 759–763.
48. **Rajab, A., et al.** 2010. Fatal cardiac arrhythmia and long-QT syndrome in a new form of congenital generalized lipodystrophy with muscle rippling (CGL4) due to PTRF-CAVIN mutations. PLoS Genet. **6:**e1000874.
49. **Razani, B., et al.** 2002. Caveolin-1-deficient mice are lean, resistant to diet-induced obesity, and show hypertriglyceridemia with adipocyte abnormalities. J. Biol. Chem. **277:**8635–8647.
50. **Razani, B., et al.** 2001. Caveolin-1 null mice are viable but show evidence of hyperproliferative and vascular abnormalities. J. Biol. Chem. **276:**38121–38138.
51. **Rim, J. S., B. Xue, B. Gawronska-Kozak, and L. P. Kozak.** 2004. Sequestration of thermogenic transcription factors in the cytoplasm during development of brown adipose tissue. J. Biol. Chem. **279:**25916–25926.
52. **Rumi, M. A., et al.** 2004. Peroxisome proliferator-activated receptor gamma-dependent and -independent growth inhibition of gastrointestinal tumour cells. Genes Cells **9:**1113–1123.
53. **Sato, H., et al.** 2000. Expression of peroxisome proliferator-activated receptor (PPAR)gamma in gastric cancer and inhibitory effects of PPARgamma agonists. Br. J. Cancer **83:**1394–1400.
54. **Schlegel, A., C. Wang, B. S. Katzenellenbogen, R. G. Pestell, and M. P. Lisanti.** 1999. Caveolin-1 potentiates estrogen receptor alpha (ERalpha) signaling. caveolin-1 drives ligand-independent nuclear translocation and activation of ERalpha. J. Biol. Chem. **274:**33551–33556.
55. **Sharma, C., A. Pradeep, R. G. Pestell, and B. Rana.** 2004. Peroxisome proliferator-activated receptor gamma activation modulates cyclin D1 transcription via beta-catenin-independent and cAMP-response element-binding protein-dependent pathways in mouse hepatocytes. J. Biol. Chem. **279:** 16927–16938.
56. **Shimada, T., et al.** 2007. Peroxisome proliferator-activated receptor gamma (PPARgamma) regulates trefoil factor family 2 (TFF2) expression in gastric epithelial cells. Int. J. Biochem. Cell Biol. **39:**626–637.
57. **Simha, V., and A. Garg.** 2009. Inherited lipodystrophies and hypertriglyceridemia. Curr. Opin. Lipidol. **20:**300–308.
58. **Stremmel, W., L. Pohl, A. Ring, and T. Herrmann.** 2001. A new concept of cellular uptake and intracellular trafficking of long-chain fatty acids. Lipids **36:**981–989.
59. **Thompson, J., et al.** 2000. A transgenic mouse line that develops early-onset invasive gastric carcinoma provides a model for carcinoembryonic antigen-targeted tumor therapy. Int. J. Cancer **86:**863–869.
60. **van Beekum, O., V. Fleskens, and E. Kalkhoven.** 2009. Posttranslational modifications of PPAR-gamma: fine-tuning the metabolic master regulator. Obesity (Silver Spring) **17:**213–219.
61. **von Knethen, A., et al.** 2007. PPARgamma1 attenuates cytosol to membrane translocation of PKCalpha to desensitize monocytes/macrophages. J. Cell Biol. **176:**681–694.
62. **von Knethen, A., N. Tzieply, C. Jennewein, and B. Brune.** 2010. Casein-kinase-II-dependent phosphorylation of PPARgamma provokes CRM1-mediated shuttling of PPARgamma from the nucleus to the cytosol. J. Cell Sci. **123:**192–201.
63. **Wainberg, Z. A., et al.** 2010. Lapatinib, a dual EGFR and HER2 kinase inhibitor, selectively inhibits HER2-amplified human gastric cancer cells and is synergistic with trastuzumab in vitro and in vivo. Clin. Cancer Res. **16:** 1509–1519.
64. **Wang, H., L. Qiang, and S. R. Farmer.** 2008. Identification of a domain within peroxisome proliferator-activated receptor gamma regulating expression of a group of genes containing fibroblast growth factor 21 that are selectively repressed by SIRT1 in adipocytes. Mol. Cell. Biol. **28:**188–200.
65. **Wei, S., et al.** 2008. A novel mechanism by which thiazolidinediones facilitate the proteasomal degradation of cyclin D1 in cancer cells. J. Biol. Chem. **283:**26759–26770.
66. **Xing, X., et al.** 2009. Hematopoietically expressed homeobox is a target gene of farnesoid X receptor in chenodeoxycholic acid-induced liver hypertrophy. Hepatology **49:**979–988.
67. **Xu, W., et al.** 2010. PPARgamma polymorphisms and cancer risk: a meta-analysis involving 32,138 subjects. Oncol. Rep. **24:**579–585.
68. **Yuasa, Y.** 2003. Control of gut differentiation and intestinal-type gastric carcinogenesis. Nat. Rev. Cancer **3:**592–600.